The DNA Single-Strand Break Repair Machinery Facilitates CAF-1-Mediated Histone Deposition at Oxidative DNA Strand Breaks

Arman Nabatiyan[1†], Zhihong Zeng and Keith W. Caldecott

Genome Damage and Stability Centre, University of Sussex, Falmer, Brighton, UK

[1]Corresponding author: Arman@Northwestern.edu, Tel: (1) 847-467-0660

[†] Present Address: Department of Biomedical Engineering, Northwestern University, 2145 Sheridan Rd, Evanston IL 60208, USA

Summary

Oxidative DNA single strand breaks arise continuously in cells and defects in their repair have been implicated in neurological disease. While much progress has been made in understanding how chromosomal single strand breaks are repaired little is known about the changes chromatin structure that accompany this process. Here, we show that nascent recombinant histone H3.1 protein accumulates and is deposited into chromatin at sites of DNA strand breakage in quiescent human cells following oxidative stress, and that core components of the single-strand break repair machinery are required for this process. We show that the SSBR sensor and scaffold proteins poly (ADP-ribose) polymerase and XRCC1 facilitate accumulation of chromatin assembly factor-1 (CAF-1) at sites of oxidative DNA strand breakage, which in turn mediates the deposition of Histone H3.1. We also demonstrate that depletion of CAF-1 slows global rates of DNA strand break repair in quiescent cells following oxidative stress, demonstrating that single-strand break repair and histone deposition are tightly co-ordinated processes. These data describe a novel role for the DNA single-strand break repair machinery and implicate histone turnover as a core component of the cellular response of quiescent cells to oxidative damage.

Introduction

DNA single strand breaks (SSBs) are the commonest type of DNA damage arising endogenously in cells, occurring at a frequency of tens-of-thousands per cell, per day. SSBs can arise directly, through attack of dexyribose by reactive oxygen species during oxidative stress, or indirectly as normal intermediates of DNA base excision repair. If not repaired, SSBs with

abnormal 3'-termini such as those induced during oxidative stress may block transcription (Zhou and Doetsch, 1994). The removal of chromosomal SSBs is normally a very rapid process that is accelerated by the SSB sensor protein poly ADP-ribose polymerase-1 (PARP-1) and the single-strand break repair (SSBR) scaffold protein XRCC1 (Caldecott, 2006; D'Amours et al., 1999; Thompson and West, 2000). PARP-1 is rapidly activated at sites of DNA strand breakage resulting in poly ADP-ribosylation of specific acceptor proteins and of itself. One role of activated PARP-1 is to promote the rapid accumulation of XRCC1 at sites of DNA strand breakage, through protein-protein and protein-ADP-ribose interactions (Caldecott et al., 1996; Masson et al., 1998), and chemical inhibition or genetic disruption of PARP-1 retards or prevents this process (El-Khamisy et al., 2003; Lan et al., 2004; Okano et al., 2003). XRCC1, in turn, then interacts with and sequesters enzymatic components of the SSBR process, and in some cases stimulates their activity. Consequently, loss of PARP-1 or XRCC1 reduces global rates of chromosomal SSBR.

Recently, mutations in Aprataxin and TDP1, two components of SSBR that interact with or are physically associated with XRCC1 (Caldecott, 2003; Clements et al., 2004; Date et al., 2004; El-Khamisy et al., 2005; Gueven et al., 2004; Plo et al., 2003), have been associated with hereditary neurodegenerative disease (Date et al., 2001; Moreira et al., 2001) . These observations implicate a crucial role for the SSBR machinery in maintaining normal neurological function, a notion consistent with the observation that the nervous system encounters particularly high levels of oxidative stress. In addition, post-mitotic cells most likely lack alternative mechanisms of removing SSBs, such as the ability to channel them into DNA double strand break repair once they have been converted into DSBs during DNA replication. Consequently, quiescent cells such as post-mitotic neurons may be particularly dependent on SSBR for chromosomal DNA integrity.

Whilst much is known about the mechanisms by which oxidative DNA single strand breaks are repaired little is known about the changes in chromatin structure that accompany this process. However, in quiescent human EJ30 bladder carcinoma cells, XRCC1 was recently shown to co-localize with chromatin assembly factor-1 (CAF-1) at sites of DNA damage induced by bleocin (Nabatiyan et al., 2006), and similar results have been reported in other cell types at sites of laser-induced UV damage (Lan et al., 2004; Okano et al., 2003). CAF-1 is a histone chaperone that is required for the deposition of histone H3.1 during chromosomal DNA replication (Hoek and Stillman, 2003; Tagami et al., 2004; Takami et al., 2006; Verreault et al., 1996; Ye et al., 2003). However, the observations described above raise the possibility that CAF-1 might also function in post-mitotic cells at DNA single strand breaks. Here, we demonstrate that this is indeed the case. We show that CAF-1 mediates deposition of histone H3.1 in quiescent human cells at sites of oxidative DNA strand breakage, and that this process is facilitated by poly (ADP-ribose) polymerase activity and by the scaffold protein XRCC1. These data demonstrate a conceptually novel role for the SSBR machinery in quiescent cells and implicate histone turnover as an integral component of the response of quiescent cells to oxidative stress.

Results

To examine whether CAF-1 might be required for the response of quiescent cells to chromosomal SSBs, we first compared levels of CAF-1 and SSBR factors in quiescent human EJ30 cell extracts before and after treatment with H_2O_2, a physiologically relevant oxidising agent that induces primarily DNA base damage and DNA single-strand breaks. Western blotting of whole cell extracts revealed that the p150 and p60 subunits of CAF-1 were rapidly and dramatically up-regulated in response to oxidative stress, and similar results

were observed for a second chromatin assembly factor, Asf-1 (Fig.1A, lanes 1-4). Intriguingly, levels of PARP-1 and XRCC1 also greatly increased in EJ30 cells following H_2O_2. In contrast, levels of the DNA replication protein PCNA were unaffected by H_2O_2 treatment. It should be noted that whilst chromatin assembly factors and SSBR proteins were greatly up-regulated following H_2O_2 treatment, longer autoradiographic exposures than those shown here revealed that these proteins were present in untreated cells (data not shown).

Notably, the up-regulated proteins were present largely in the insoluble protein fraction of quiescent EJ30 cells because they required 0.3-0.5 M NaCl for extraction, suggesting a tight association with chromatin (Fig.1B&C, lanes 1-4). We also noted that the up-regulation of XRCC1, CAF-1, Asf-1, and PARP-1 by oxidative stress was reduced by ~half by pre-incubation with PARP inhibitor, suggesting that this event was promoted by PARP activity (Fig.1A, lanes 5-8), and a corresponding reduction was observed in the amount of these proteins in the chromatin fractions (Fig.1B&C, compare lanes 1-4 with 5-8). These data indicate that chromatin assembly factors and core components of the SSBR machinery are both up-regulated in quiescent EJ30 cells in response to oxidative stress, and that this response is promoted by PARP activity.

At the concentration of inhibitor employed, synthesis of poly ADP-ribose (PAR) is greatly reduced or absent (data not shown and see Fig.2A, panels ii & iv).

We have shown previously that sites of H_2O_2-induced PAR synthesis co-localize extensively with sites of XRCC1 accumulation (El-Khamisy et al., 2003; Rogakou et al., 1999; Rogakou et al., 1998), consistent with the observation that the majority (>99%) of breaks induced by H_2O_2 are SSBs (Bradley and Kohn, 1979). We therefore compared the sub-cellular localization of CAF-1 with sites of poly ADP-ribose (PAR) synthesis in H_2O_2-treated EJ30 cells, to examine whether the chromatin assembly machinery

accumulates at oxidative SSBs. Although the co-localization of CAF-1 with sites of PAR synthesis has been observed following laser-induced UV DNA damage (Lan et al., 2004; Okano et al., 2003), it was important to determine whether this relationship exists at physiologically relevant SSBs. Strikingly, within 15 min following H_2O_2 treatment, the p60 subunit of CAF-1 accumulated into nuclear foci that were brighter and more punctate than those present before treatment, and these foci co-localized extensively with sites of PAR synthesis (Fig.2A, compare panels i & ii). The intensity of both PAR and CAF-1 signals declined within 30 min after H_2O_2 treatment, and the co-localization of these molecules was lost, consistent with the rapidity of SSBR (Fig.2A, compare panels ii & iii). Interestingly, we noted that CAF-1 accumulation following H_2O_2 was weaker and less punctate in EJ30 cells that were pre-treated with PARP inhibitor at concentration that greatly reduced or ablated PAR synthesis (Fig.2A, compare panels ii & iv). We also noted that only a small subset of H_2O_2-induced CAF-1 sites co-localized with sites of γ-H2AX, a marker of DSBs (El-Khamisy et al., 2003; Rogakou et al., 1999; Rogakou et al., 1998), ,consistent with CAF-1 accumulation occurring primarily at SSBs (Fig.2B). Together, these data indicate that CAF-1 accumulates at sites of chromosomal DNA single strand breaks following oxidative stress, in a dynamic manner that parallels the kinetics of, and is promoted by, PAR synthesis.

One role of PARP-1 at SSBs is to sequester XRCC1, a molecular scaffold protein that interacts with multiple enzymatic components of the SSBR process and facilitates their accumulation at SSBs (El-Khamisy et al., 2003; Lan et al., 2004; Okano et al., 2003). Consequently, we examined whether XRCC1 was required for accumulation of CAF-1 at oxidative SSBs. Strikingly, siRNA-mediated depletion of XRCC1 reduced the intensity of CAF-1 p60 foci and largely prevented their co-localization with sites of PAR synthesis (Fig.2C, Panel ii). We noted that XRCC1 depletion also reduced the extent of PAR

synthesis in these experiments. This may reflect an indirect effect of XRCC1 on the length of PAR polymer synthesized at SSBs, since XRCC1 binds PAR directly (Pleschke et al., 2000). In contrast to XRCC1 depletion, parallel control experiments employing luciferase siRNA had no effect on either CAF1 p60 accumulation or PAR synthesis following H_2O_2 (Fig.2C, Panel i). These experiments indicate that the accumulation of CAF-1 at sites of chromosomal SSBs requires the SSBR scaffold protein XRCC1.

Given the results described above, we examined whether CAF-1 physically associates with the SSBR machinery. Consistent with this notion, immunoprecipitation CAF-1 p150 co-recovered XRCC1 both before and after H_2O_2 treatment, suggesting that these proteins were constitutively associated (Fig.2D, lanes 2-5). In contrast, XRCC1 was not detected in a control immunoprecipitation conducted with anti-HA antibodies in parallel (Fig.2D, lane 1). We did not detect CAF-1 in the anti-CAF-1 p150 immunoprecipitates before H_2O_2 treatment, most likely due to the very low levels of these proteins present prior to H_2O_2 treatment (e.g. see Fig. 1A). However, CAF-1 p60 was detected in CAF-1 immunoprecipitates 15-30 minutes after H_2O_2 treatment, when CAF-1 levels were much higher (Fig.2D, lanes 4 & 5). We noted that PARP-1 was also immunoprecipitated by anti-CAF-1 p150 antibodies following H_2O_2 treatment, consistent with the co-association of XRCC1 and PARP-1 with CAF-1 following oxidative stress (Fig.2D, lanes 4 & 5).

What role might CAF-1 play at SSBs following oxidative stress? In light of the results described above we considered the possibility that CAF-1 may facilitate the turnover or deposition of histones in quiescent cells in response to oxidative stress, and that this process might be facilitated by the SSBR machinery. To examine this hypothesis, we examined whether transiently-transfected GFP-tagged histone H3.1 was incorporated into the salt-resistant fraction of quiescent EJ30 nuclei following treatment with H_2O_2. In the absence of H_2O_2 treatment, in most GFP-positive cells (~75%) the GFP signal

was pan-nuclear, weak, and diffuse (e.g. see Fig.3A, panel I), whereas in the remaining cells (~25%) the GFP signal was pan-nuclear and very intense (data not shown). More importantly, whilst the frequency of transfected cells with very intense pan-nuclear GFP did not change following oxidative stress, the majority (~65%) of the transfected cells acquired a very striking focal pattern of GFP staining within 15 min after H_2O_2 treatment (Fig.3A, panel II). Moreover, the GFP foci in these cells largely (>90%) co-localized with sites of CAF-1 accumulation, suggesting that these foci reflected CAF-1-mediated deposition of GFP-H3.1 into chromatin. Consistent with this notion, the sites of GFP-H3.1 accumulation induced by H_2O_2 were also resistant to extraction with detergent (Fig.3A, panels III & IV), and were sensitive to treatment with DNaseI (Fig.3B, left panel). We noted in the latter case that in some cells (~5%) partial DNAseI digestion was observed, resulting in some residual centres of DAPI staining (Fig.3B, right panel). Residual GFP signal was clearly present at many of these regions of undigested DNA, further demonstrating that the recombinant histone was chromatin-associated.

We considered it unlikely that these data reflected replication-associated deposition of GFP-H3.1, in a residual sub-population of S phase EJ30 cells, for two reasons. First, the focal deposition of GFP-H3.1 in the 'quiescent' populations of EJ30 cells employed here was entirely dependent on treatment with H_2O_2. In contrast, BrdUrd pulse labeling experiments revealed that GFP-H3.1 deposition was readily detected in the absence of H_2O_2 in actively proliferating cultures of EJ30 cells (Fig.3C, left panels). Second, pulse labeling also revealed that less than 4% of the EJ30 cells in the 'quiescent' populations employed in these experiments were in S phase (data not shown), yet ~65% of the GFP-transfected cells deposited GFP-H3.1 into chromatin following H_2O_2-treatment. Indeed, these experiments confirmed that H_2O_2-induced deposition of GFP-H3.1 in 'quiescent' populations EJ30 cells occurred in cells that were not undergoing chromosomal DNA

replication (Fig. 3C, right panels). To rule out that the GFP-H3.1 deposition following oxidative stress was a phenomenon restricted to EJ30 cells we employed MCF7 breast carcinoma cells, which we rendered quiescent by treatment with the estrogen receptor antagonist, ICI 182780 (Polo et al., 2004). As observed in EJ30 cells, CAF-1 accumulated into foci that co-localized with sites of GFP-H3.1 deposition in quiescent MCF7 cells, in response to oxidative stress (Fig.4A). Moreover, the deposition of GFP-H3.1 again occurred in cells that were not undergoing chromosomal DNA replication (Fig.4B).

As an alternative technique for measuring GFP-H3.1 deposition following oxidative stress we employed biochemical fractionation. Cells transfected with pEGFP-H3.1 or with unrelated empty vector (pBEND3) were separated into a soluble cytoplasmic protein fraction and a fraction containing nuclear and cytoskeletal material. The nuclear and cytoskeletal material was then sequential extracted with 0.3-1M NaCl, and cell-equivalent aliquots of each of the soluble protein fractions examined for the presence of GFP-H3.1 by immunoblotting with anti-GFP and anti-H3 antibodies. Surprisingly, in cells immediately after H_2O_2 treatment (before SSBR and CAF-1 accumulation occur), anti-GFP antibodies detected a polypeptide of ~25 kDa in the nuclear/cytoskeletal protein fractions (Fig. 4C, top panel, lanes 6-8). This polypeptide was absent from cells transfected with an unrelated control plasmid, confirming that it was a product of the GFP ORF in pEGFP-H3.1 (Fig.4C, top panel, lanes 2-4). We noted that the molecular mass of this polypeptide was consistent with it being GFP lacking the H3.1 moiety and, indeed, anti-histone H3 antibody failed to detect this polypeptide, despite detecting native histone H3 migrating at ~15 kDa (Fig.4C, bottom panel, lanes 6-8). Consequently, we conclude that this product reflects a derivative of GFP-H3.1 in which the H3 moiety has been removed.

Strikingly, fifteen minutes after H_2O_2 treatment, anti-GFP antibodies detected a polypeptide of ~42 kDa in the nuclear/cytoskeletal material, which

is the molecular mass expected for full-length GFP-H3.1 protein (Fig.4C, top panel, lanes 10-12). This polypeptide was also detected by anti-histone H3 antibodies, confirming that it contained both GFP and histone H3 moieties (Fig.4C, bottom panel, lanes 10-12). Moreover, this protein required 0.5-1M salt for efficient extraction, consistent with its tight association with chromatin (Fig.4C, top and bottom panels, lanes 10-12). Interestingly, concomitant with the appearance of GFP-H3.1, we noted that the level of truncated (~25 kDa) GFP polypeptide lacking histone H3 was greatly decreased or absent fifteen minutes after H_2O_2 treatment, suggesting that the recombinant histone was 'protected' from degradation in response to oxidative stress (Fig.4C, bottom panel, lanes 10-12).

To define the mechanism by which GFP-H3.1 is deposited into chromatin at sites of oxidative single strand breakage, we examined whether deposition of GFP-H3.1 was prevented by depletion of CAF-1 and XRCC1. Whereas quiescent EJ30 cells transfected with control luciferase siRNA exhibited robust GFP-H3.1 deposition (Fig.5, panels 1&2), the level of GFP-H3.1 deposition was greatly reduced in cells transfected with CAF-1 p60 siRNA (Fig.5A, panels 3&4). Moreover, similar results were observed in EJ30 cells that were either transfected with XRCC1 siRNA (Fig.5A, panels 5&6) or pre-treated with PARP inhibitor (Fig.5A, panel 7). In the latter two cases, as observed previously (see Fig.1A & 1C), CAF-1 accumulation was less punctate than in normal cells, and in addition failed to co-localize with GFP-H3.1. Together, these data demonstrate that both CAF-1 and core components of the SSBR machinery are required for efficient deposition of GFP-H3.1 following oxidative stress.

Having demonstrated that the SSBR machinery is critical for efficient deposition of GFP-H3.1 into chromatin at sites of oxidative SSBs, we next examined whether the histone deposition machinery is important for SSBR. We thus employed single-cell alkaline agarose gel electrophoresis (Comet)

assays to measure the global rate of SSBR in the quiescent EJ30 cells depleted of either CAF-1 (p150) or Asf-1, a second chromatin assembly factor, or mock-depleted with luciferase siRNA (Fig.6A). In addition, we employed EJ30 cells depleted of XRCC1 as a positive control. H_2O_2 induced similar initial levels of single-strand breakage in each of the cell lines (Fig.6B, middle bars). However, in cells in which either XRCC1 or CAF-1 p150 was depleted the global rate of SSBR was reduced (Fig.6B, right bars). A mild repair defect was also observed in the Asf1 depleted cells, but this was not statistically significant. The SSBR defect in CAF-1 depleted cells was apparent not only from the mean tail moments from multiple experiments, but also from the distribution of tail moments within individual populations of cells (Fig.6C). These data indicate that CAF-1 is required for rapid global rates of chromosomal SSBR in quiescent EJ30 cells.

Discussion

The results presented here demonstrate that CAF-1-mediated histone deposition is an integral component of the cellular response to oxidative stress in quiescent cells and that this process is closely co-ordinated with enzymatic steps of chromosomal single-strand break repair (SSBR). These findings are significant for several reasons. First, they describe a conceptually novel role for the SSBR machinery, demonstrating that core components of this process facilitate not only the repair of chromosomal DNA but also the metabolism of chromosomal proteins. Second, since tens of thousands of chromosomal SSBs arise per cell per day, these data imply that histone turnover is a continuous event even in cells that are not undergoing DNA replication, challenging the concept that these proteins are rarely if ever replaced in post-mitotic cells. Third, these data identify, for the first time, a

functional role for CAF-1 and the chromatin assembly machinery in non-replicating cells.

Levels of CAF-1 are down-regulated in a variety of cells once they enter quiescence, including EJ30 cells, most likely because extensive deposition of histones during DNA replication is no longer required (Nabatiyan et al., 2006; Polo et al., 2004). Intriguingly, however, we observed that levels of both critical chromatin assembly factors and SSBR proteins were dramatically up-regulated in quiescent EJ30 cells following treatment with H_2O_2. Thus, whilst residual levels of chromatin assembly and SSBR proteins may be sufficient for histone turnover in response to the continuous but low basal level of oxidative stress in untreated quiescent cells, an up-regulation of these factors in response to acutely elevated levels oxidative stress is most likely required to increase the cellular capacity for histone turnover. The nature of the mechanism/s by which CAF-1 and SSBR components are up-regulated in these cells is unknown, and is an exciting area for future study.

Detectable levels of GFP-tagged histone H3.1 were present in the chromatin of quiescent EJ30 cells within fifteen minutes after H_2O_2 treatment, as measured by direct fluorescence microscopy. Full-length GFP-H3.1 was also detected in these cells in biochemical fractionation experiments, and the requirement for 0.5-1M NaCl for efficient extraction of the GFP-H3.1 from the nuclear/cytoskeletal material is consistent with its tight association with chromatin. In contrast, detectable levels of full-length GFP-tagged histone H3.1 were absent from quiescent EJ30 cells immediately after H_2O_2 treatment. Rather, we detected the presence of a smaller GFP molecule that lacked the histone moiety, most of which was soluble at concentrations of NaCl below 0.5M. These data suggest that in the absence of oxidative stress GFP-H3.1 is degraded, but that following oxidative stress this molecule becomes 'protected', either to allow its deposition into chromatin or by the deposition event itself. This, in turn, raises the exciting possibility that quiescent cells

possess a potent mechanism for regulating levels of excess unincorporated histone.

Recently, it was demonstrated that CAF-1 also facilitates histone deposition at sites of nucleotide excision repair (NER), following exposure to ultraviolet light (Polo et al., 2006). Whilst UV damage is not relevant to most cells in vivo, together, these studies suggest that histone turnover may be an integral component of most, if not all, DNA repair pathways. Interestingly, whereas CAF-1 depletion reduced rates of SSBR in the current study, it did not measurably impact on the rate of NER following UV irradiation (Polo et al., 2006). This may indicate that histone turnover is more tightly integrated with the SSBR process than it is with NER. It is not yet clear why CAF-1 depletion inhibits chromosomal SSBR. One possibility is that loss of CAF-1 also impacts on the removal of histones at SSBs, in addition to their subsequent replacement. A failure to remove or displace histones from sites of SSBs may impede the repair process, particularly those DNA end-processing and/or gap-filling events conducted by DNA polymerase β (Beard et al., 2003; Caldecott, 2006). Alternatively, it is possible that histone turnover and SSBR are so tightly integrated that disruption of the former also disrupts the latter. The observation that nucleosome reassembly can be initiated at DNA gaps in vitro, before the DNA repair event is completed, is consistent with this idea (Green and Almouzni, 2003; Moggs et al., 2000).

What is the mechanism by which SSBR and histone turnover are integrated? The deposition of GFP-H3.1 at oxidative SSBs required both PAR synthesis and the molecular scaffold protein, XRCC1. PAR synthesis is triggered by the binding of PARP-1 and/or PARP-2 to DNA strand breaks, one consequence of which is the accumulation of XRCC1 at the break (Caldecott, 2006). XRCC1, in turn, interacts with and recruits/accumulates enzymatic components of the SSBR process, and in some cases stimulates their activity. In light of our data, we suggest that the accumulation CAF-1 at

sites of oxidative SSBs is facilitated in a similar manner, via the association of CAF-1 with XRCC1 reported here, thereby enabling the deposition of histone H3.1. It will be of interest to examine the relationship between the SSBR machinery and other histone chaperones since, presumably, other histones are also metabolised at oxidative SSBs.

It is not yet clear why histone deposition occurs following oxidative stress. One possibility is that histone turnover is a stochastic process that occurs as a consequence of displacing histones from the nucleosome during SSBR. Alternatively, since reactive oxygen species can oxidize proteins in addition to DNA, it is possible that coupling histone deposition to chromosomal SSBR prevents the accumulation of oxidised histones in chromatin, thereby maintaining epigenetic stability in long-lived cells, such as post-mitotic neurons.

Materials and Methods

Cell culture. Human EJ30 bladder carcinoma cells (a kind gift from T.Krude) were cultured as monolayers in Dulbecco's modified Eagle's medium supplemented with 1g/L glucose (note; low glucose), Glutamax, 10% fetal calf serum, 10 units/ml penicillin, 0.1 mg/ml streptomycin, and 2.5 μg/ml amphotericin B (Fungizone) (all from Gibco BRL). Cells were made quiescent by cultivation to confluence followed by incubation in medium supplemented with 0.5% fetal calf serum for 7 to 10 days (Krude, 1999). MCF7 cells were cultivated in DMEM supplemented with 15% serum and brought into quiescence with application (10nM) of the estrogen receptor antagonist ICI 182,780 (Tocris Bioscience) for 48h.

Antibodies. The primary antibodies employed for these experiments were anti-PAR Mab 10H (Alexis), anti-PARP-1 Mab A6.4.7 (kindly provided by Dr.

Said Aoufouchi; now available from Serotec as clone A6.4.12), anti-βActin Mab AC-40 (Sigma), anti-Asf1 a/b polyclonal antibody (Groth et al., 2005), anti-XRCC1 Mab 33-2-5, anti-γ-H2AX Mab JBW301 (Upstate Technologies), anti-CAF-1 p60 polyclonal pAb1 (Marheineke and Krude, 1998), anti-CAF-1 p150 Mab (SS-1) (Smith and Stillman, 1991), anti-histone H3 polyclonal antibody (Abcam; ab1791), anti-BrdU Mab B44 (Becton Dickinson) and anti-HA Mab 12CA5 (Cancer Research UK), and anti-GFP Mab (Roche;11814460001).

DNA-damaging agents and inhibitors. Quiescent cells were treated with the indicated concentration of H_2O_2 in PBS on ice for 10 min and then incubated for the indicated repair-period at 37°C in drug-free media. Where relevant, 1μM PARP inhibitor (KU-58948; KuDOS Pharmaceutical) in PBS was applied prior to (overnight) and throughout the experiment.

Salt Fractionation of Cells. Cells were incubated in ice-cold hypotonic buffer (20mM HEPES-KOH, 5mM KCl, 1.5mM $MgCl_2$, 1mM DTT) for 10 min to promote swelling and then ruptured by 10 passages through a 29G needle. Nuclei and insoluble cytoskeletal material was pelleted at 5000 rpm for 2 min in a microfuge and the supernatant containing soluble cytoplasmic protein was retained. Nuclei and cytoskeletal material were re-suspended in ice-cold 'hypotonic' buffer containing 150mM (for experiments in Figure 1) or 300mM (for experiments in Figure 4) NaCl by brief vortexing and incubated on ice for 30 min. Insoluble nuclear and cytoskeletal material was pelleted at 10,000 rpm for 2 min and the supernatant retained. Proteins were then sequentially extracted from the insoluble nuclear and cytoskeletal material, as described above, with cold 'hypotonic' buffer containing either 0.3M and 0.5M NaCl (for experiments in Figure 1), or 0.5M and 1M NaCl (for experiments in Figure 4). Aliquots of each soluble protein fraction ($3x10^6$ cell equivalents) were

fractionated by SDS-PAGE, transferred to nitrocellulose, and immunoblotted with the antibodies indicated.

Fluorescence Microscopy. Indirect immunofluorescence microscopy was performed as detailed elsewhere (Szuts and Krude, 2004). For salt fractionation of 'intact' cells, cells grown on coverslips were chilled on ice, washed in PBS, and incubated in ice-cold hypotonic buffer (20mM HEPES-KOH, 5mM KCl, 1.5mM $MgCl_2$, 0.01% Triton, 1mM DTT) for 5 min. The buffer was then replaced with ice-cold buffer of the same composition but additionally containing 150mM NaCl for a further 10 min on ice. For detergent extraction, coverslips were treated with ice-cold PBS containing 0.2% Triton-X100 for 5 min on ice. Cells were then fixed with 4% paraformaldehyde prior to immunostaining with the antibodies indicated. Pulse labeling with 50 μM BrdU was conducted for 1.5 h. After fixation, cellular DNA was treated with 1M HCl on ice for 30 min prior to immunodetection. Images were captured on a LSM 510 at 63X magnification. DNAseI treatment was performed as described previously (Martini et al., 1998)

siRNA-mediated silencing and transient-transfection of GFP-H3. For siRNA-mediated depletion of specific proteins, EJ30 cells were grown in 6-well plates to 50-70% confluence and then incubated in media containing low-serum (see above) for 24 hr prior to transfection. Transfections were conducted using Lipofectamine 2000 (Invitrogen) in DMEM lacking serum, antibiotics and fungizone. The double stranded siRNA for CAF-1 p60 (Nabatiyan and Krude, 2004), CAF-1 p150 (Hoek and Stillman, 2003), Asf1 a/b (Groth et al., 2005), and Luciferase (Hoek and Stillman, 2003) were obtained from Dharmacon and have been described previously. The siRNA for XRCC1 was obtained from Qiagen (SI02665117). All siRNAs were applied at a final concentration of 150 nM and a media change was performed 4-6 hr after

transfection to reduce cytotoxicity. Samples were harvested for analysis 72 hr after transfection. For transfection of GFP-H3.1, the same protocol was followed except that cells were seeded at a density of 30-40% and transfections were performed using 6.5μg of pEGFP-H3.1 per $1x10^6$ cells, 72 hr after serum starvation. pEGFP-H3.1 was generated by sub-cloning PCR-amplified H3.1 ORF into pEGFPC3 (Clonetech).

Comet assays. Comet assays were performed as described elsewhere (Breslin et al., 2006)

Immunoprecipitation assays. Whole cell extracts were prepared by re-suspension of untreated and H_2O_2-treated cells in ice-cold isotonic buffer (150mM NaCl, 20mM HEPES-KOH, 5mM KCl, 1.5mM $MgCl_2$, 1mM DTT). Cells were sonicated briefly on ice (3x10s bursts at 25% amplitude) and the concentration of soluble protein determined using the Bradford assay. 25 μg of either anti-CAF-1 p150 antibody anti-HA tag antibody was added to aliquots of cell extract (5 mg total protein) and incubated on a roller wheel at 4°C overnight. 50 μl of Protein G beads (Cancer Research UK) were then added and incubation continued for 2 hr at 4°C. Antibody complexes were pelleted in a microfuge, washed with ice-cold isotonic buffer (3x1 ml), re-suspended in 2XSDS loading buffer, fractionated by SDS-PAGE, and transferred to nitrocellulose for immunoblotting.

Figure Legends

Fig.1. Induction and chromatin association of SSBR proteins and chromatin assembly factors in quiescent EJ30 cells following oxidative stress.
(A) Whole-cell extracts (50 μg total protein) from untreated cells ("Unt") or from H_2O_2-treated cells (150 μM) after 0 min, 15 min, or 30 min recovery in

drug-free medium, as indicated, were analyzed by Western blotting using antibodies specific for the p150 and p60 subunits of CAF-1, Asf1a/b, PCNA, PARP-1, or XRCC1, as indicated. Ponceau S total-protein staining and anti-β Actin antibodies were employed to confirm equal protein loading. Where indicated ("+PARPi"), cells were pre-treated with PARP inhibitor. **(B&C)** Quiescent EJ30 cells pre-incubated or not with PARP inhibitor, as indicated, were treated with 150μM H_2O_2 and incubated for 15 min (B) or 30 min (C) in drug-free media to allow time for repair. Cells were then fractionated into a soluble cytoplasmic protein fraction ("Cyt.") and into three nuclear/cytoskeletal ("Nuc/CSK") fractions created by sequential extraction of the nuclear and cytoskeletal pellet with 0.15M, 0.3M, and 0.5M NaCl, as indicated. Aliquots (3 x 10^6 cell equivalents) of each fraction were fractionated by SDS-PAGE and immunoblotted with antibodies against the indicated proteins.

Fig.2. XRCC1-dependent recruitment of CAF-1 at chromsomal DNA strand breaks following oxidative stress. **(A)** Quiescent EJ30 cells were mock-treated ("-H_2O_2") or treated with 10mM H_2O_2 for 10 min on ice followed by incubation in drug-free medium for 15 or 30 min, as indicated. Sites of PAR synthesis (red) and CAF-1 p60 accumulation (green) were detected in salt-extracted (150mM NaCl) nuclei by confocal immunofluorescence microscopy. Where indicated, cells were pre-incubated with PARP inhibitor ("+PARPi") prior to and during treatment with H_2O_2. **(B)** Sites of γ-H2AX (green) and CAF-1 p60 accumulation (red) were detected in quiescent EJ30 cells treated as described above. **(C)**, Quiescent EJ30 cells were treated with 10mM H_2O_2 for 10 min on ice followed by incubation in drug-free medium for 15 min. Sites of PAR synthesis (red) and CAF-1 p60 accumulation (green) were detected in salt-extracted (150mM NaCl) nuclei by confocal immunofluorescence microscopy. Where indicated, cells were pre-incubated with luciferase ("Luc")

or XRCC1 siRNA prior to treatment with H_2O_2. Note that in Panels A-C, representative images are presented. **(D)**, Sonicated whole-cell extracts (5 mg total protein) from untreated ("Unt") or H_2O_2-treated (150μM) quiescent EJ30 cells, pre-incubated (+PARPi) or not with 1 μM PARP inhibitor, were immunoprecipitated with 25 μg of either CAF-1 p150 or anti-HA tag Mab. Antibody complexes were fractionated by SDS-PAGE and immunoblotted for the indicated proteins. An aliquot of the input sample from the IP shown in lane 4 is included for reference. Note that the difference in electrophoretic mobility between the immunoprecipitated proteins and input proteins in these experiments reflects the high concentrations of IgG and/or sepharose in the precipitates. The PARP-1 band with retarded mobility in lane 4 (asterisk) is auto-ribosylated PARP.

Fig.3. XRCC1-mediated deposition of GFP-tagged histone H3.1 at sites of oxidative DNA strand breakage. **(A)** Quiescent EJ30 cells were transiently transfected with pEGFP- H3.1 and 24 hr later mock-treated or treated with 10 mM H_2O_2. Sites of CAF-1 p60 accumulation (red) were detected in salt-extracted (150mM NaCl; Panels I & II) or Triton-X100-extracted (0.2%; Panels III & IV) cells using anti-p60 antibody and GFP-H3.1 deposition (green) was detected by direct fluorescence microscopy. **(B)** Quiescent populations of pEGFP-H3.1-transfected EJ30 cells were extracted with Triton-X100 and mock-treated or treated with DNase I prior to or 15 min after treatment with H_2O_2, as above. CAF-1 p60 (red) and GFP-H3.1 (green) was detected as described above and DNA was counterstained with DAPI (blue). Note that the cell depicted in the left and right panels show the impact of complete and partial DNaseI digestion, respectively. **(C),** Proliferating ("Prolif.") or quiescent populations of pEGFP-H3.1-transfected EJ30 cells were pulse labeled with BrdUrd for 1.5 h and sites of BrdU incorporation (red) and GFP-

H3.1 deposition (green) detected in cells prior to or 15 min after treatment with H_2O_2, as above. In all panels, representative images are presented.

Fig.4. (A), Quiescent populations of pEGFP-H3.1-transfected MCF7 cells were mock-treated or treated with 10 mM H_2O_2 and sites of CAF-1 p60 (red) and GFP-H3.1 (green) detected in salt-extracted (150mM NaCl) cells as described above. **(B)**, Quiescent populations of pEGFP-H3.1-transfected MCF7 cells were pulse labeled with BrdUrd for 1.5 h and sites of BrdU incorporation (red) and GFP-H3.1 (green) detected in cells prior to or 15 min after treatment with 150 μM H_2O_2. Representative images are presented in the panels above. **(C),** Quiescent EJ30 cells transfected with pEGFP-H3.1 or with unrelated pBEND3 vector were fractionated, either immediately after H_2O_2 treatment or following a 15 min repair period, into a soluble cytoplasmic protein fraction ("Cyt.") and into three nuclear/cytoskeletal ("Nuc/CSK") fractions created by sequential extraction of the nuclear and cytoskeletal pellet with 0.3M, 0.5M, and 1M NaCl, as indicated. Aliquots (3×10^6 cell equivalents) of each fraction were fractionated by SDS-PAGE and immunoblotted with antibodies against the indicated proteins.

Fig.5. Quiescent populations of pEGFP-H3.1-transfected EJ30 cells were mock-treated or treated with 10 mM H_2O_2 and sites of CAF-1 p60 (red) and GFP-H3.1 (green) detected in salt-extracted (150mM NaCl) cells as described above. Where indicated, cells were pre-incubated with luciferase ("Luc"), CAF-1 (p60), or XRCC1 siRNA, or with PARP inhibitor. Representative images are presented. Note that whereas the level of CAF-1 p60 depletion is shown in Panel 4, levels of XRCC1 depletion are shown in Fig.6A.

Fig.6. (A) Quiescent EJ30 cells (1×10^6) were transfected with luciferase control siRNA ("cont.") or with siRNA directed against either XRCC1, Asf1 a/b or

CAF-1 p150 ("target") and levels of the targeted protein (indicated on the left) assessed 72-hr later by immunoblotting. Note that β-Actin levels are inlcuded as loading controls. **(B)** DNA strand breakage was measured by the alkaline Comet assay in quiescent EJ30 cells treated as above either immediately after H_2O_2-treatment (75 μM for 10 min on ice) or after subsequent 15 min incubation in drug-free medium. Data are the average tail moment of 100 cells per sample and are the mean of this value (+/- 1 SD) from four independent experiments. **(C)** Representative scatter plots showing the raw data from one of the experiments used in Panel B. These data show the distribution of individual tail moments (Y-axis) within each population of 100 cells. Each cell is numbered from 1-100 (X-axis).

References

Beard, B. C., Wilson, S. H., and Smerdon, M. J. (2003). Suppressed catalytic activity of base excision repair enzymes on rotationally positioned uracil in nucleosomes. Proc Natl Acad Sci U S A *100*, 7465-7470.

Bradley, M. O., and Kohn, K. W. (1979). X-ray induced DNA double strand break production and repair in mammalian cells as measured by neutral filter elution. Nucleic Acids Res *7*, 793-804.

Breslin, C., Clements, P. M., El-Khamisy, S. F., Petermann, E., Iles, N., and Caldecott, K. W. (2006). Measurement of chromosomal DNA single-strand breaks and replication fork progression rates. Methods Enzymol *409*, 410-425.

Caldecott, K. W. (2003). DNA single-strand break repair and spinocerebellar ataxia. Cell *112*, 7-10.

Caldecott, K. W. (2006). Mammalian single-strand break repair: Mechanisms and links with chromatin. DNA Repair (Amst).

Caldecott, K. W., Aoufouchi, S., Johnson, P., and Shall, S. (1996). XRCC1 polypeptide interacts with DNA polymerase beta and possibly poly (ADP-ribose) polymerase, and DNA ligase III is a novel molecular 'nick-sensor' in vitro. Nucleic Acids Res *24*, 4387-4394.

Clements, P. M., Breslin, C., Deeks, E. D., Byrd, P. J., Ju, L., Bieganowski, P., Brenner, C., Moreira, M. C., Taylor, A. M., and Caldecott, K. W. (2004). The

ataxia-oculomotor apraxia 1 gene product has a role distinct from ATM and interacts with the DNA strand break repair proteins XRCC1 and XRCC4. DNA Repair (Amst) *3*, 1493-1502.

D'Amours, D., Desnoyers, S., D'Silva, I., and Poirier, G. G. (1999). Poly(ADP-ribosyl)ation reactions in the regulation of nuclear functions. Biochem J *342 (Pt 2)*, 249-268.

Date, H., Igarashi, S., Sano, Y., Takahashi, T., Takahashi, T., Takano, H., Tsuji, S., Nishizawa, M., and Onodera, O. (2004). The FHA domain of aprataxin interacts with the C-terminal region of XRCC1. Biochem Biophys Res Commun *325*, 1279-1285.

Date, H., Onodera, O., Tanaka, H., Iwabuchi, K., Uekawa, K., Igarashi, S., Koike, R., Hiroi, T., Yuasa, T., Awaya, Y.*, et al.* (2001). Early-onset ataxia with ocular motor apraxia and hypoalbuminemia is caused by mutations in a new HIT superfamily gene. Nat Genet *29*, 184-188.

El-Khamisy, S. F., Masutani, M., Suzuki, H., and Caldecott, K. W. (2003). A requirement for PARP-1 for the assembly or stability of XRCC1 nuclear foci at sites of oxidative DNA damage. Nucleic Acids Res *31*, 5526-5533.

El-Khamisy, S. F., Saifi, G. M., Weinfeld, M., Johansson, F., Helleday, T., Lupski, J. R., and Caldecott, K. W. (2005). Defective DNA single-strand break repair in spinocerebellar ataxia with axonal neuropathy-1. Nature *434*, 108-113.

Green, C. M., and Almouzni, G. (2003). Local action of the chromatin assembly factor CAF-1 at sites of nucleotide excision repair in vivo. Embo J *22*, 5163-5174.

Groth, A., Ray-Gallet, D., Quivy, J. P., Lukas, J., Bartek, J., and Almouzni, G. (2005). Human Asf1 regulates the flow of S phase histones during replicational stress. Mol Cell *17*, 301-311.

Gueven, N., Becherel, O. J., Kijas, A. W., Chen, P., Howe, O., Rudolph, J. H., Gatti, R., Date, H., Onodera, O., Taucher-Scholz, G., and Lavin, M. F. (2004). Aprataxin, a novel protein that protects against genotoxic stress. Hum Mol Genet *13*, 1081-1093.

Hoek, M., and Stillman, B. (2003). Chromatin assembly factor 1 is essential and couples chromatin assembly to DNA replication in vivo. Proc Natl Acad Sci U S A *100*, 12183-12188.

Krude, T. (1999). Mimosine arrests proliferating human cells before onset of DNA replication in a dose-dependent manner. Exp Cell Res *247*, 148-159.

Lan, L., Nakajima, S., Oohata, Y., Takao, M., Okano, S., Masutani, M., Wilson, S. H., and Yasui, A. (2004). In situ analysis of repair processes for oxidative DNA damage in mammalian cells. Proc Natl Acad Sci U S A *101*, 13738-13743.

Marheineke, K., and Krude, T. (1998). Nucleosome assembly activity and intracellular localization of human CAF-1 changes during the cell division cycle. J Biol Chem *273*, 15279-15286.

Martini, E., Roche, D. M., Marheineke, K., Verreault, A., and Almouzni, G. (1998). Recruitment of phosphorylated chromatin assembly factor 1 to chromatin after UV irradiation of human cells. J Cell Biol *143*, 563-575.

Masson, M., Niedergang, C., Schreiber, V., Muller, S., Menissier-de Murcia, J., and de Murcia, G. (1998). XRCC1 is specifically associated with poly(ADP-ribose) polymerase and negatively regulates its activity following DNA damage. Mol Cell Biol *18*, 3563-3571.

Moggs, J. G., Grandi, P., Quivy, J. P., Jonsson, Z. O., Hubscher, U., Becker, P. B., and Almouzni, G. (2000). A CAF-1-PCNA-mediated chromatin assembly pathway triggered by sensing DNA damage. Mol Cell Biol *20*, 1206-1218.

Moreira, M. C., Barbot, C., Tachi, N., Kozuka, N., Uchida, E., Gibson, T., Mendonca, P., Costa, M., Barros, J., Yanagisawa, T.*, et al.* (2001). The gene mutated in ataxia-ocular apraxia 1 encodes the new HIT/Zn-finger protein aprataxin. Nat Genet *29*, 189-193.

Nabatiyan, A., and Krude, T. (2004). Silencing of chromatin assembly factor 1 in human cells leads to cell death and loss of chromatin assembly during DNA synthesis. Mol Cell Biol *24*, 2853-2862.

Nabatiyan, A., Szuts, D., and Krude, T. (2006). Induction of CAF-1 expression in response to DNA strand breaks in quiescent human cells. Mol Cell Biol *26*, 1839-1849.

Okano, S., Lan, L., Caldecott, K. W., Mori, T., and Yasui, A. (2003). Spatial and temporal cellular responses to single-strand breaks in human cells. Mol Cell Biol *23*, 3974-3981.

Pleschke, J. M., Kleczkowska, H. E., Strohm, M., and Althaus, F. R. (2000). Poly(ADP-ribose) binds to specific domains in DNA damage checkpoint proteins. JBiolChem *275*, 40974-40980.

Plo, I., Liao, Z. Y., Barcelo, J. M., Kohlhagen, G., Caldecott, K. W., Weinfeld, M., and Pommier, Y. (2003). Association of XRCC1 and tyrosyl DNA phosphodiesterase (Tdp1) for the repair of topoisomerase I-mediated DNA lesions. DNA Repair (Amst) *2*, 1087-1100.

Polo, S. E., Roche, D., and Almouzni, G. (2006). New Histone Incorporation Marks Sites of UV Repair in Human Cells. Cell *127*, 481-493.

Polo, S. E., Theocharis, S. E., Klijanienko, J., Savignoni, A., Asselain, B., Vielh, P., and Almouzni, G. (2004). Chromatin assembly factor-1, a marker of clinical value to distinguish quiescent from proliferating cells. Cancer Res *64*, 2371-2381.

Rogakou, E. P., Boon, C., Redon, C., and Bonner, W. M. (1999). Megabase chromatin domains involved in DNA double-strand breaks in vivo. J Cell Biol *146*, 905-916.

Rogakou, E. P., Pilch, D. R., Orr, A. H., Ivanova, V. S., and Bonner, W. M. (1998). DNA double-stranded breaks induce histone H2AX phosphorylation on serine 139. J Biol Chem *273*, 5858-5868.

Smith, S., and Stillman, B. (1991). Immunological characterization of chromatin assembly factor I, a human cell factor required for chromatin assembly during DNA replication in vitro. J Biol Chem *266*, 12041-12047.

Szuts, D., and Krude, T. (2004). Cell cycle arrest at the initiation step of human chromosomal DNA replication causes DNA damage. J Cell Sci *117*, 4897-4908.

Tagami, H., Ray-Gallet, D., Almouzni, G., and Nakatani, Y. (2004). Histone H3.1 and H3.3 complexes mediate nucleosome assembly pathways dependent or independent of DNA synthesis. Cell *116*, 51-61.

Takami, Y., Ono, T., Fukagawa, T., Shibahara, K. I., and Nakayama, T. (2006). Essential Role of CAF-1-mediated Rapid Nucleosome Assembly for DNA Replication and Cell Division in Vertebrate Cells. Mol Biol Cell.

Thompson, L. H., and West, M. G. (2000). XRCC1 keeps DNA from getting stranded. Mutat Res *459*, 1-18.

Verreault, A., Kaufman, P. D., Kobayashi, R., and Stillman, B. (1996). Nucleosome assembly by a complex of CAF-1 and acetylated histones H3/H4. Cell *87*, 95-104.

Ye, X., Franco, A. A., Santos, H., Nelson, D. M., Kaufman, P. D., and Adams, P. D. (2003). Defective S phase chromatin assembly causes DNA damage, activation of the S phase checkpoint, and S phase arrest. Mol Cell *11*, 341-351.

Zhou, W., and Doetsch, P. W. (1994). Transcription bypass or blockage at single-strand breaks on the DNA template strand: effect of different 3' and 5' flanking groups on the T7 RNA polymerase elongation complex. Biochem *33*, 14926-14934.

Figure 1

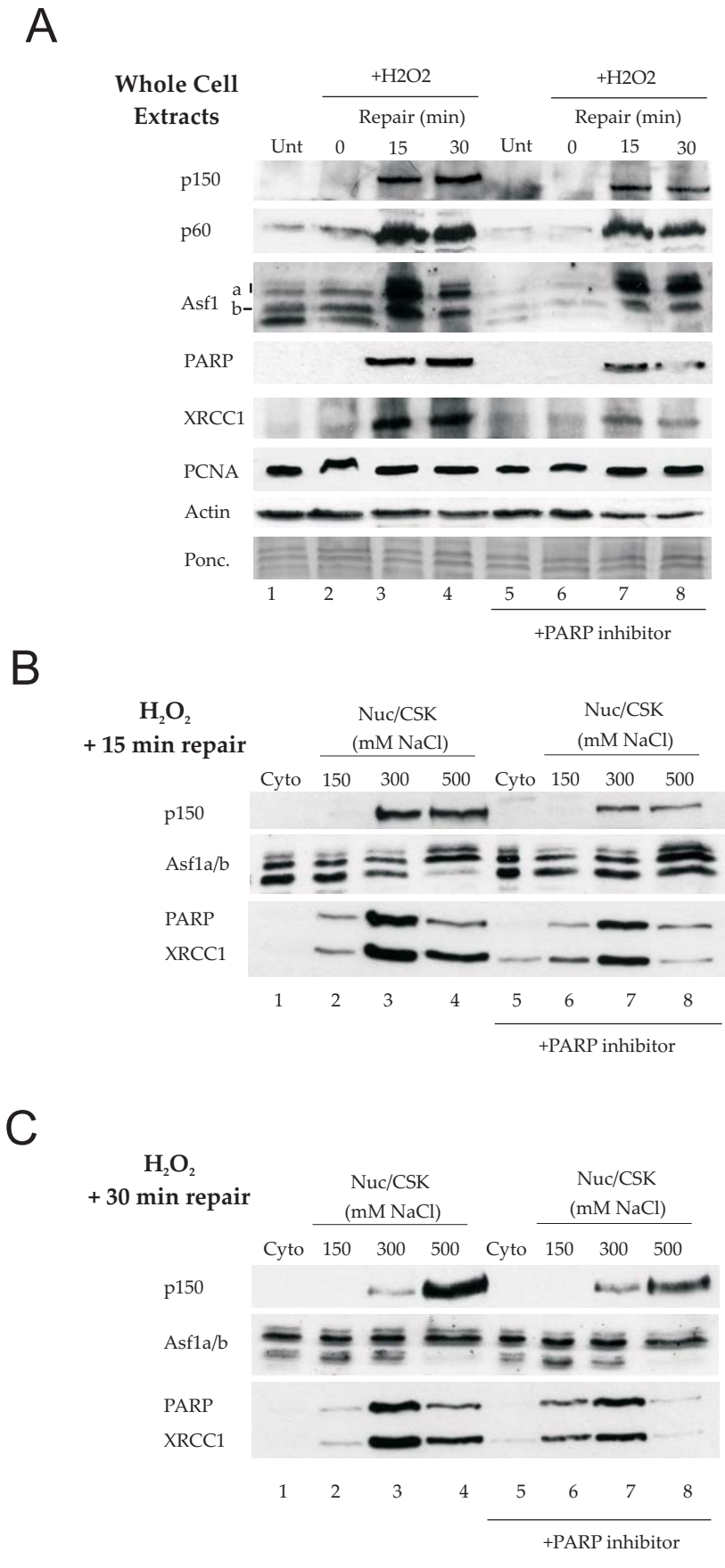
A
Whole Cell Extracts
+H2O2
+H2O2
Repair (min)
Repair (min)
Unt 0 15 30 Unt 0 15 30
p150
p60
Asf1 a b
PARP
XRCC1
PCNA
Actin
Ponc.
1 2 3 4 5 6 7 8
+PARP inhibitor
B
H2O2 + 15 min repair
Nuc/CSK (mM NaCl)
Nuc/CSK (mM NaCl)
Cyto 150 300 500 Cyto 150 300 500
p150
Asf1a/b
PARP
XRCC1
1 2 3 4 5 6 7 8
+PARP inhibitor
C
H2O2 + 30 min repair
Nuc/CSK (mM NaCl)
Nuc/CSK (mM NaCl)
Cyto 150 300 500 Cyto 150 300 500
p150
Asf1a/b
PARP
XRCC1
1 2 3 4 5 6 7 8
+PARP inhibitor

Figure 2

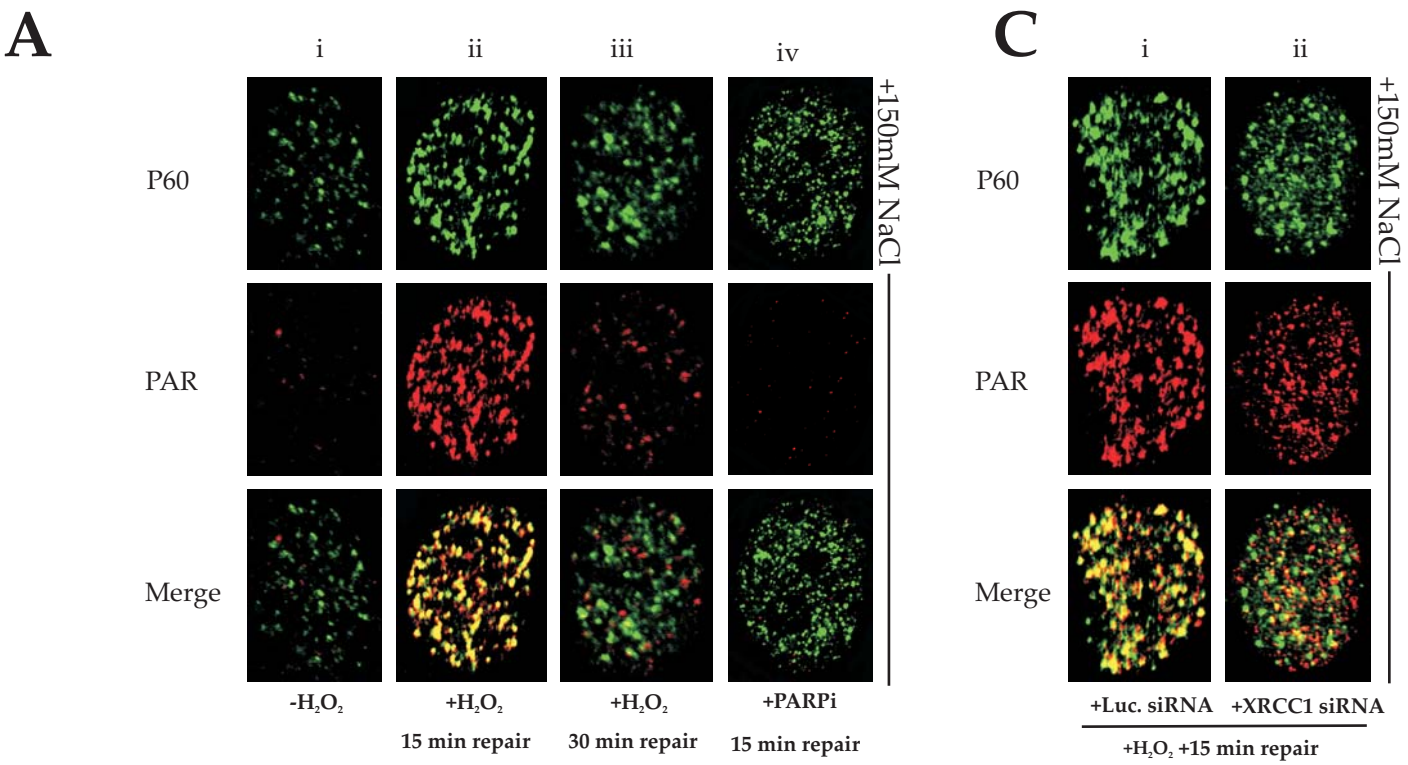
A
i
ii
iii
iv
P60
PAR
Merge
+150mM NaCl
-H2O2
+H2O2
15 min repair
+H2O2
30 min repair
+PARPi
15 min repair
C
i
ii
P60
PAR
Merge
+150mM NaCl
+Luc. siRNA
+XRCC1 siRNA
+H2O2 +15 min repair

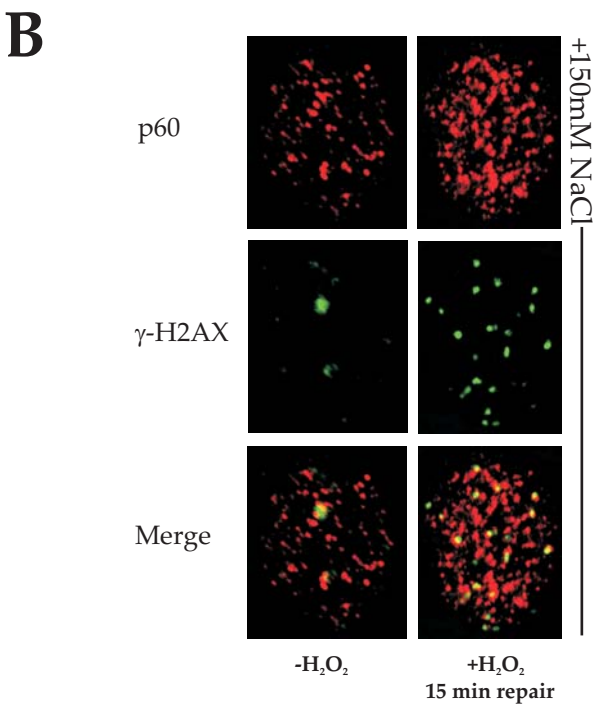
B
p60
γ-H2AX
Merge
+150mM NaCl
-H2O2
+H2O2
15 min repair

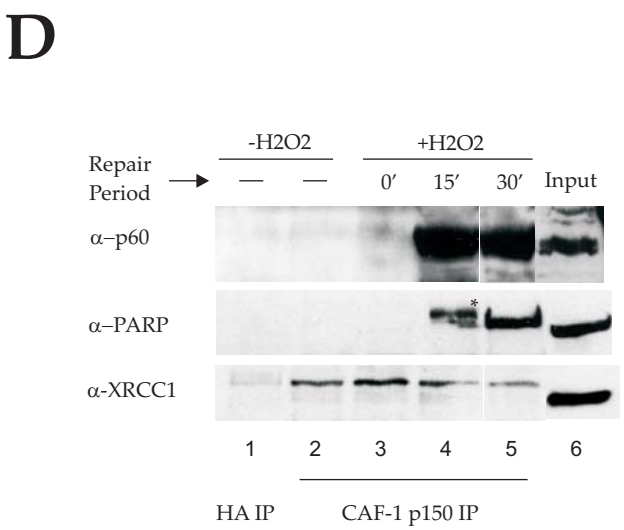
D
-H2O2
+H2O2
Repair Period
0′
15′
30′
Input
α–p60
α–PARP
α-XRCC1
1
2
3
4
5
6
HA IP
CAF-1 p150 IP

Figure 3

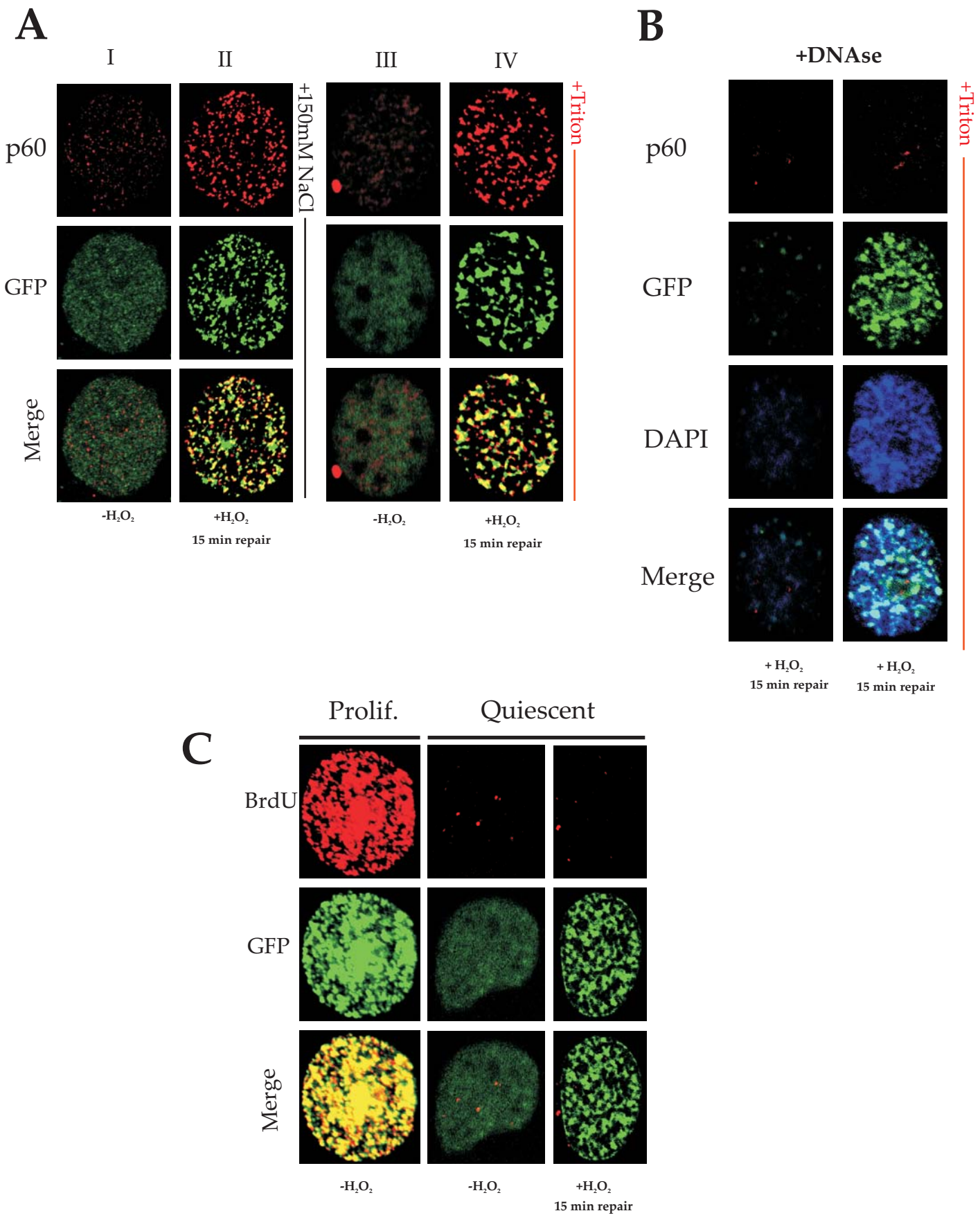
A
I
II
III
IV
p60
GFP
Merge
+150mM NaCl
+Triton
-H2O2
+H2O2
15 min repair
-H2O2
+H2O2
15 min repair
B
+DNAse
p60
GFP
DAPI
Merge
+Triton
+ H2O2
15 min repair
+ H2O2
15 min repair
C
Prolif.
Quiescent
BrdU
GFP
Merge
-H2O2
-H2O2
+H2O2
15 min repair

Figure 4

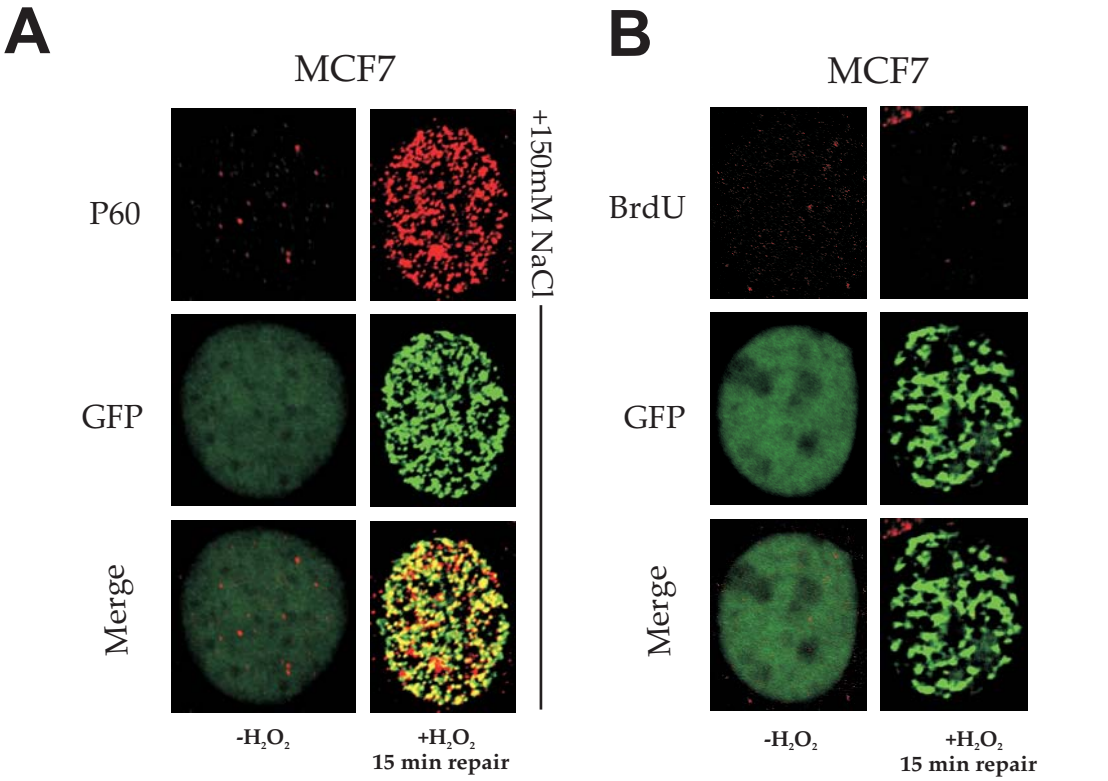
A
MCF7
P60
GFP
Merge
+150mM NaCl
-H2O2
+H2O2
15 min repair
B
MCF7
BrdU
GFP
Merge
-H2O2
+H2O2
15 min repair

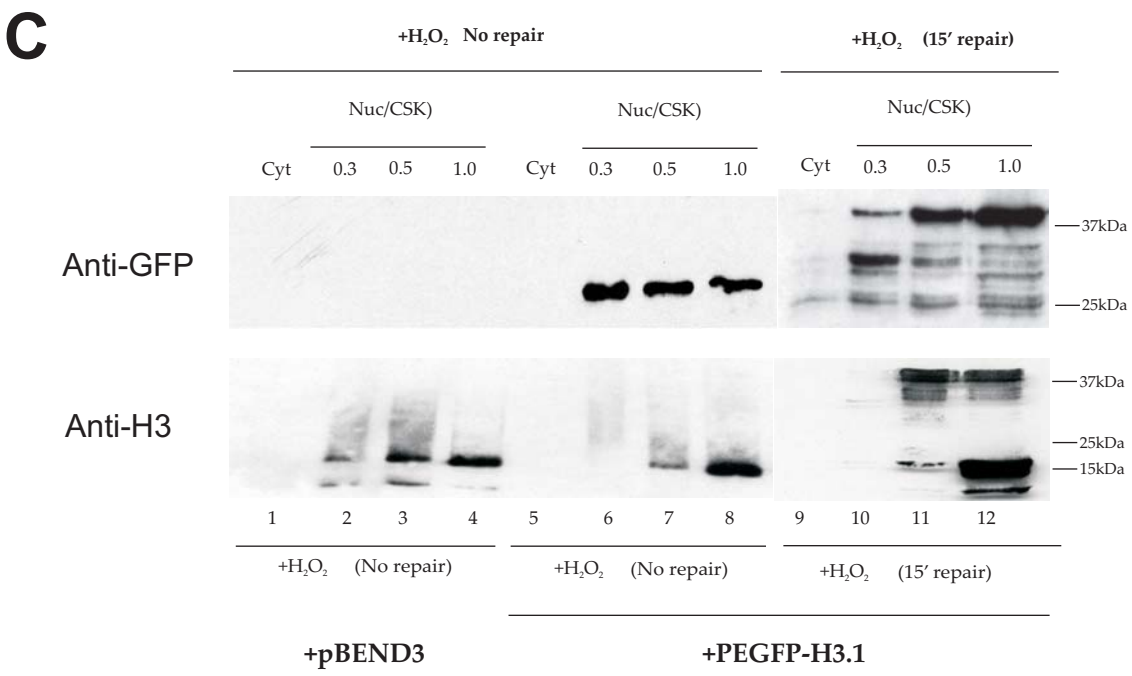
C
+H2O2 No repair
+H2O2 (15′ repair)
Nuc/CSK)
Cyt 0.3 0.5 1.0
Anti-GFP
Anti-H3
37kDa
25kDa
15kDa
1 2 3 4 5 6 7 8 9 10 11 12
+H2O2 (No repair)
+H2O2 (No repair)
+H2O2 (15′ repair)
+pBEND3
+PEGFP-H3.1

Figure 5

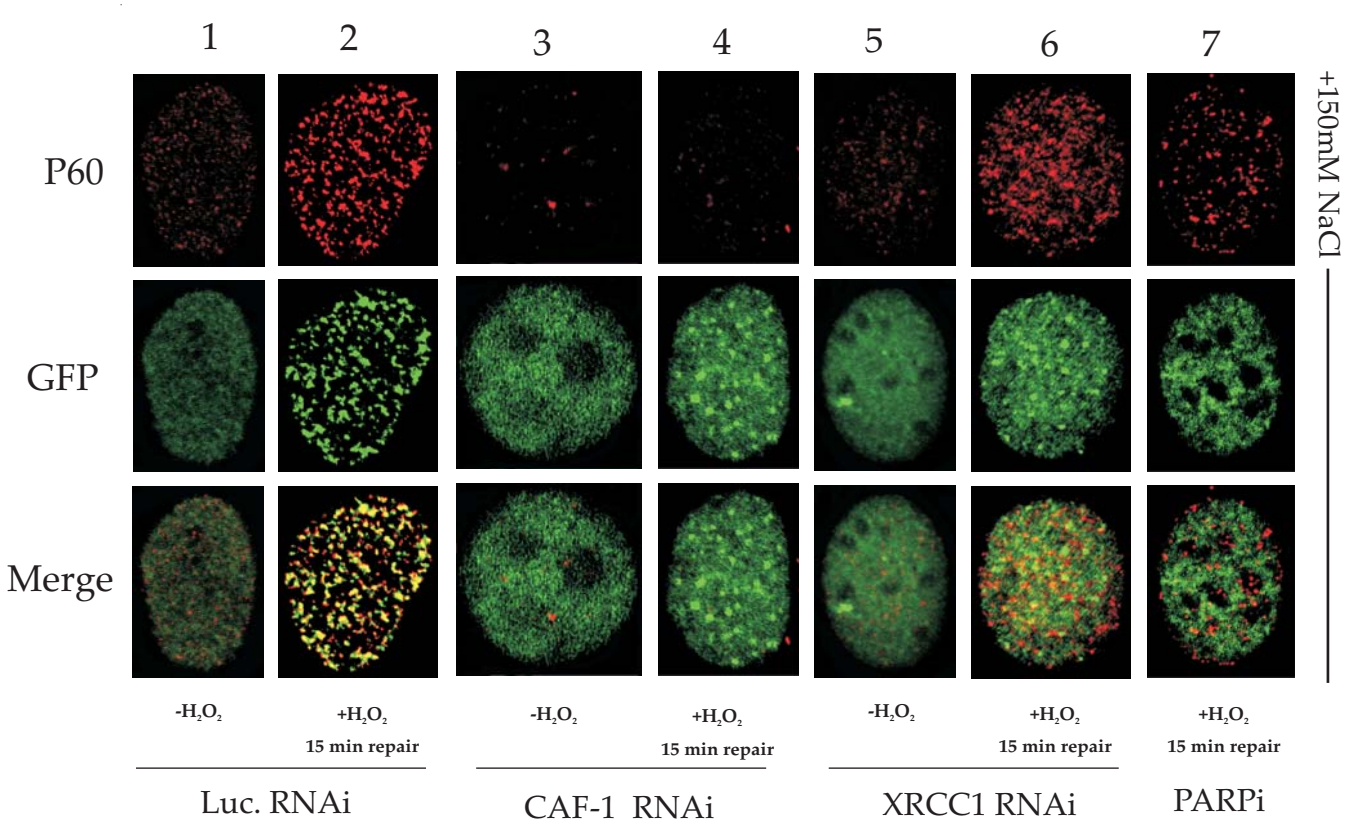
1
2
3
4
5
6
7
P60
GFP
Merge
+150mM NaCl
-H2O2
+H2O2
15 min repair
-H2O2
+H2O2
15 min repair
-H2O2
+H2O2
15 min repair
+H2O2
15 min repair
Luc. RNAi
CAF-1 RNAi
XRCC1 RNAi
PARPi

Figure 6

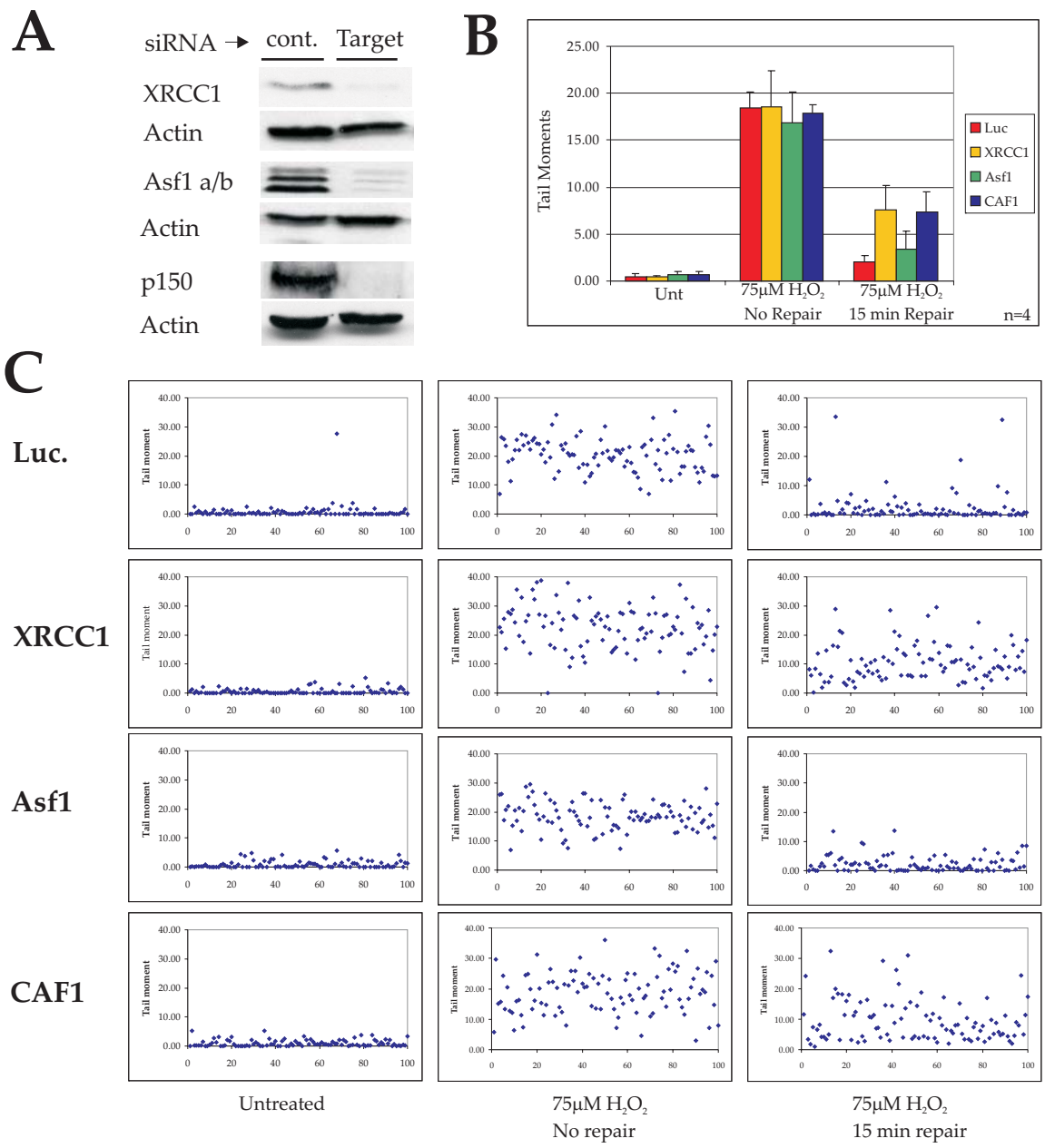
A
siRNA → cont. Target
XRCC1
Actin
Asf1 a/b
Actin
p150
Actin
B
Tail Moments
25.00
20.00
15.00
10.00
5.00
0.00
Luc
XRCC1
Asf1
CAF1
Unt
75μM H2O2 No Repair
75μM H2O2 15 min Repair
n=4
C
Luc.
XRCC1
Asf1
CAF1
Tail moment
Untreated
75μM H2O2 No repair
75μM H2O2 15 min repair